

Separating aerodynamic from acoustic-induced velocity on a portion of an acoustic liner through modal decomposition methods

*Original*

Separating aerodynamic from acoustic-induced velocity on a portion of an acoustic liner through modal decomposition methods / Scarano, Francesco; Lyu, Benshuai; Paduano, Angelo; Avallone, Francesco. - 766:(2025), pp. 5423-5430. ( Forum Acusticum Euronoise 2025. 11th Convention of the European Acoustics Association Malaga (ESP) 23-26 June 2025) [10.61782/fa.2025.0766].

*Availability:*

This version is available at: 11583/3001529 since: 2025-07-04T07:03:27Z

*Publisher:*

EAA

*Published*

DOI:10.61782/fa.2025.0766

*Terms of use:*

This article is made available under terms and conditions as specified in the corresponding bibliographic description in the repository

*Publisher copyright*

(Article begins on next page)



# FORUM ACUSTICUM EURONOISE 2025

## SEPARATING AERODYNAMIC FROM ACOUSTIC-INDUCED VELOCITY ON A PORTION OF AN ACOUSTIC LINER THROUGH MODAL DECOMPOSITION METHODS

Francesco Scarano<sup>1\*</sup>

Benshuai Lyu<sup>2</sup>

Angelo Paduano<sup>1</sup>

Francesco Avallone<sup>1</sup>

<sup>1</sup> Department of Mechanical and Aerospace Engineering (DIMEAS), Politecnico di Torino, Italy

<sup>2</sup> College of Engineering, Peking University, China

### ABSTRACT

The separation of acoustic-induced velocity from the turbulent velocity fluctuations is tackled on a numerical database representing a segment of an acoustic liner subjected to a grazing acoustic wave and a turbulent grazing flow. The evaluation of the acoustic velocity in the current test case has practical implications for the liner's impedance calculation and sound absorption properties. The separation of the acoustic induced velocity from the turbulent fluctuation is provided by modal decomposition methods: proper orthogonal decomposition (POD), spectral proper orthogonal decomposition (SPOD) and the recently developed canonical correlation decomposition (CCD). For all the decomposition methods, the capability to decompose the acoustic and the aerodynamic component is affected the amplitude of the acoustic waves with respect to the background turbulence. The CCD and SPOD are found to outperform POD when the acoustic amplitude is low compared with the background turbulence. For SPOD, the acoustic forcing frequency needs to be known a-priori or easily identifiable in the spectrum to correctly filter out the acoustic induced velocity. POD and CCD have the advantage of automatically capture non-linear effects due to the vortex shedding which are associated with high order modes.

\*Corresponding author: francesco.scarano@polito.it.

Copyright: ©2025 F. Scarano et al. This is an open-access article distributed under the terms of the Creative Commons Attribution 3.0 Unported License, which permits unrestricted use, distribution, and reproduction in any medium, provided the original author and source are credited.

**Keywords:** *aeroacoustics, acoustic liners, acoustic velocity, modal decomposition methods*

### 1. INTRODUCTION

In computational aeroacoustics or during time-resolved measurements in turbulent fields, instantaneous pressure or velocity signals capture both aerodynamic fluctuations and acoustic disturbances. These aerodynamic and acoustic components are coupled, yet separating them is essential for understanding their interaction [1].

The pseudo-sound or aerodynamic component is often weakly influenced by compressibility [2], while the acoustic component is governed by sound wave propagation. The acoustic velocity can either result from unsteady turbulence, as it happens for turbulent jets [3], or due to an external acoustic source. In the first context, the acoustic velocity field is crucial for understanding sound generation and dissipation due to the turbulence.

Conversely, the latter scenario describe an acoustic wave that interacts with a turbulent flow, a meaningful example being the operating conditions of acoustic liners. The acoustic liners absorb noise in aircraft engines, they interact with grazing acoustic waves and turbulent boundary layers. The impedance, defined as the ratio of pressure to acoustic velocity, plays a key role in understanding their noise-absorbing properties. The challenge of separating these fields and the practical relevance for impedance education make the acoustic liner orifice a valuable benchmarks to separate the aerodynamic from the acoustic component.

Several methods, such as frequency-wavenumber de-





# FORUM ACUSTICUM EURONOISE 2025

composition [4], Helmholtz decomposition [5], and dynamic mode decomposition (DMD) [6], have been proposed to decompose aerodynamic and acoustic components from velocity or pressure fields. Helmholtz decomposition separates irrotational and solenoidal components, though it is computationally expensive and suited for three-dimensional, homogeneous fields. Wavelet-based techniques, developed by Grizzi et al. [7] and Mancinelli et al. [3], isolate hydrodynamic from acoustic components by exploiting the intermittent nature of hydrodynamic pressure.

This study explores modal decomposition methods for separating aerodynamic and acoustic velocity components by identifying coherent modes in the flow. Modal decomposition offers a reduced-order model for the flow, and the potential of proper orthogonal decomposition (POD), spectral proper orthogonal decomposition (SPOD), and the recently developed canonical correlation decomposition (CCD) [8] is explored to extract acoustic-driven flow structures. POD, CCD and SPOD are applied to numerical data from an acoustic liner orifice, with the goal of isolating the acoustic velocity.

## 2. DECOMPOSITION METHODS

### 2.1 Proper Orthogonal Decomposition (POD)

POD, introduced by [9], decomposes a turbulent velocity field into spatial modes that capture portions of the turbulent kinetic energy. The first step of the procedure to apply POD is based on writing the collection of  $N$  uncorrelated snapshots  $\mathbf{u}_i$  in compact matrix forms as  $\mathbf{U} = [\mathbf{u}_1, \mathbf{u}_2, \mathbf{u}_3 \dots \mathbf{u}_N]$ . Among the several methods to perform POD and extract the modes, the simplest procedure makes use of the singular value decomposition on the snapshot matrix

$$\mathbf{U}^T / \sqrt{N-1} \quad (1)$$

where  $T$  is the transpose of the matrix. For a detailed review, the reader should refer to [10] and [11].

### 2.2 Canonical Correlation Decomposition (CCD)

CCD, recently introduced by [8], decomposes the flow and rank the modes based on their correlation with a reference signal located in an observable location. The aim of the technique is to identify coherent structures correlated with the observable. The procedure involves the construction of the matrix:

$$\mathbf{A} = \frac{1}{\sqrt{QN}} \mathbf{P} \mathbf{U}^\dagger, \quad (2)$$

where  $\mathbf{P}$  is the observable matrix, and  $\mathbf{U}$  is the flow snapshot matrix and  $Q$  is the observable vector length. The CCD modes are extracted through the singular value decomposition of  $\mathbf{A}$ .

### 2.3 Spectral Proper Orthogonal Decomposition (SPOD)

SPOD combines POD with temporal coherence, isolating modes that capture both spatial and temporal correlations. The flow snapshots are first Fourier transformed using Welch's method, then the cross-spectral density matrix is computed:

$$\mathbf{S} = \frac{1}{N-1} \hat{\mathbf{U}} \hat{\mathbf{U}}^\dagger. \quad (3)$$

SPOD modes are the eigenvectors of this matrix, representing coherent structures in the flow [12].

### 2.4 Acoustic Induced Velocity Estimation

The acoustic-induced velocity is reconstructed using a reduced-order model (ROM) with the first modes:

$$\mathbf{v}_{ac}(x, y, t) \cong \sum_1^{k_n} c_k(t) \Phi_k(x, y). \quad (4)$$

where  $\Phi_k(\mathbf{x})$  are the modes and  $c_k(t)$  the temporal coefficients obtained from the decompositions. Modes are selected based on their energy, correlation, and spectral properties. In the current paper the reconstructed velocity for the POD and CCD is obtained using the first three modes ranked by energy and correlation strength. For the SPOD the acoustic velocity is reconstructed using the first mode only but providing a band pass reconstruction centred at two frequencies, the source tone and its first harmonic as shown in figure 2 (c,d). The acoustic velocity is normalized by the theoretical linear response of the Helmholtz resonator [13],  $v_{ac}^*$ , in no flow conditions which is equal to 5.76 m/s for 130 dB and 25.96 m/s for 145 dB..

## 3. NUMERICAL DATABASE AND FLOW DESCRIPTION

### 3.1 Methodology

This study builds upon the simulation database described in [14]. Simulations were conducted with 3DS Simulia



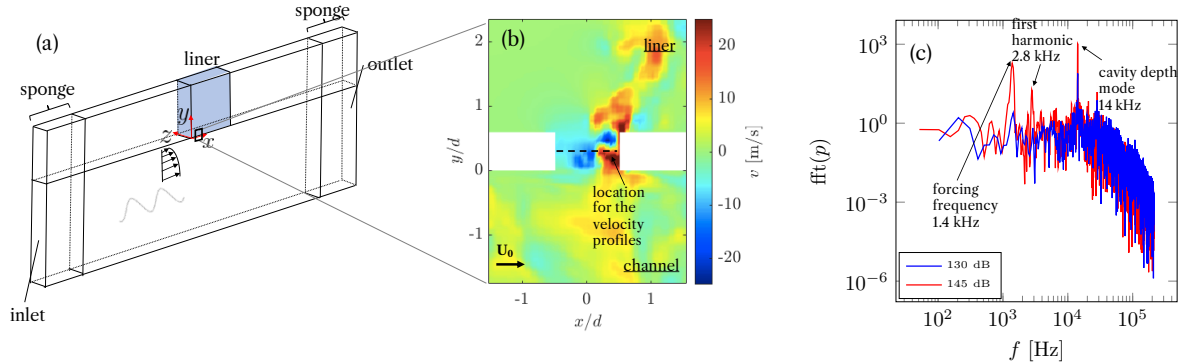


**Figure 1.** Sketch of the numerical setup (a) 3D geometry, (b) contour of the unfiltered vertical velocity fluctuation, randomly chosen snapshot for the case  $M = 0.32$  and SPL 145 dB, (c) spectrum of the pressure fluctuations in the orifice, comparison between 130 dB and 145 dB at  $M = 0.32$

PowerFLOW (v6), a solver based on the Lattice Boltzmann Method (LBM), which solves the discretized Boltzmann equation in space and time [15]. The solver uses a 3-dimensional lattice with 19 discrete velocity directions, the D3Q19 model [16]. The study adopts a very large eddy simulation (VLES) approach, which resolves large turbulence scales while modeling sub-grid scales via an effective relaxation time [17].

### 3.2 Numerical setup

The computational domain follows the setup described in [14]. The liner is positioned on the top wall of a rectangular duct, consisting of eleven cavities with square cross-sections. The dataset used for the analysis is a 2D field cropped near an orifice of the acoustic liner, as depicted in figure 1 (a) and (b). The orifice has a diameter,  $d$ , of 1.17 mm. The streamwise coordinate is  $x$ , the spanwise coordinate is  $z$ , and the vertical coordinate is  $y$ . The velocity components are  $u'$ ,  $v'$ , and  $w'$ , with their time-averaged values denoted by capital letters  $U$ ,  $V$ , and  $W$ , and the fluctuation components by lowercase  $u$ ,  $v$ , and  $w$ .

To trigger boundary layer transition, a zig-zag trip was placed upstream of the liner at  $x = -1600$  mm [18]. Quasi-anechoic conditions were achieved at the duct termination by exponentially increasing the fluid viscosity in sponge regions by a factor of 100. Periodic boundary conditions were applied along the lateral sides of the domain.

For the discretization of the domain, a variable resolution scheme was applied to the lattice grid, with six meshes in an overset arrangement. The finest grid reso-

lution was used for the facesheet, orifices, and part of the backing cavities. The minimum grid spacing in the orifice was  $\Delta z_{min} = \Delta y_{min} = \Delta x_{min} = 0.0234$  mm, resulting in an effective resolution of approximately 40 voxels/ $d$ . A mesh independence study is presented in [14].

### 3.3 Aeroacoustic description of the acoustic liner physical mechanism and numerical database description

For the current geometry, the acoustic liner absorbs and dissipates incident acoustic energy based on the principle of Helmholtz resonators. The resonant frequency of the liner without grazing flow is 1.4 kHz, which shifts to higher values in the presence of flow. Acoustic-induced flow variations within the orifice exhibit periodic modulation with varying phases, from inflow ( $\phi = \pi/2$ ) to outflow ( $\phi = 3\pi/2$ ).

The liner is subjected to a grazing flow with a Mach number of 0.32, and two different sound pressure levels (SPLs) are tested. The acoustic forcing can be observed as a peak at 1.4 kHz in the pressure signal spectrum, as shown in figure 1 (c).

The different cases tested are summarized in Table 1. Each dataset consists of 4740 snapshots with a sampling frequency of 420 kHz. A complete characterization of the aero-acoustic properties is detailed in [14].

The inclusion of two different SPL aims to capture the liner's functioning regimes. When the incident acoustic wave has a low SPL (below 130 dB), the liner operates in the linear regime, where acoustic energy is absorbed



**Table 1.** List of the simulations analysed in this work.

Mach number	SPL (dB)	Frequency (kHz)
0.32	130	1.4
0.32	145	1.4

via viscous effects [19]. At higher SPL and in presence of grazing flow, the dissipation mechanism shifts to turbulent jets and vortex shedding at the orifice openings, indicating the non-linear regime [20,21].

At  $M = 0.32$  and SPL = 145 dB, a randomly chosen snapshot of the vertical velocity fluctuation is shown in figure 1 (b). The turbulence entering the orifice disrupts the coherence of the velocity fluctuations, leading to the generation of broadband "noise." This phenomenon complicates the acoustic and aerodynamic decomposition, as it introduces additional, non-periodic components that hinder the clear separation of acoustic and aerodynamic contributions [20]. As the SPL increases from 130 to 145 dB, the acoustic-to-hydrodynamic fluctuation ratio (AHFR) increases, the pressure signal spectrum in figure 1 (c) shows increased energy at the source frequency with increasing SPL.

A second peak at 14 kHz is observed in the pressure signal spectrum inside the orifice for both SPLs, which represents a cavity depth mode associated with standing waves. This peak is more prominent in the presence of a grazing flow and corresponds to a Helmholtz resonator mode [22,23]. This high-frequency fluctuation adds to the challenge of acoustic/aerodynamic decomposition, acting as an additional sharp disturbance in the system.

## 4. RESULTS

### 4.1 Energy and correlation strength distribution between the modes and spectra

The normalized percentage of energy and correlation strength distribution between the modes for  $M = 0.32$  is shown in figure 2 (a and b). For the POD results (a), the first two modes account for less than 10% of the total energy for both SPL conditions. This is due to the presence of the turbulence close to the walls and it is further accentuated by the self-tone at 14 kHz acting as broad and sharp disturbing factors respectively in the modal decompositions. This suggests that the POD is not capable of correctly extracting the acoustic velocity associated with

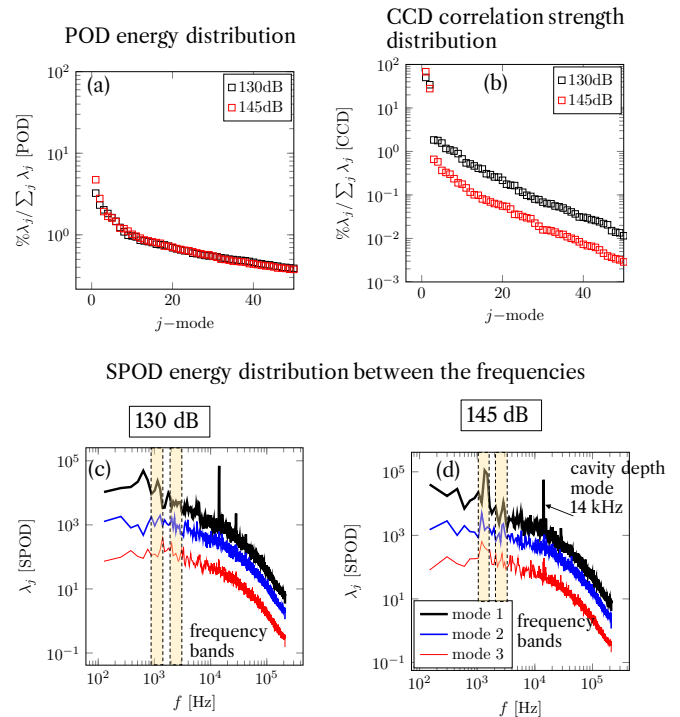


**Figure 2.** Fraction of the energy for POD (a) and correlation energy for CCD (b) between the modes, comparison between the two SPL. SPOD spectra at 130 dB (c) and 145 dB (d), results obtained with a grazing flow of  $M = 0.32$ .

the forcing frequency due to the fact that the POD modes are dominated by the significant energy associated with the 14 kHz tone. Conversely, the CCD correlation energy distribution (figure 2 (b)) exhibits a quick-decaying behaviour. In this sense, CCD is more suitable than POD in diagnosing the acoustically-driven flow since it targets the upstream forcing-correlated flow structures. The low-rank behaviour is further accentuated when the SPL is larger as the AHFR increases.

In figure 2 (c,d) the energy distribution between the frequencies for the SPOD at the two SPL studied is depicted. Contrary to POD and CCD, the SPOD spectra provide directly the modes' energetic content and the frequency distribution of each mode. For the SPOD results, the forcing frequency at 1.4 kHz, and the cavity mode at 14 kHz are highlighted in the figures along with the frequency bands used for the reconstruction which are centred at the source frequency and its first harmonic. When



# FORUM ACUSTICUM EURONOISE 2025

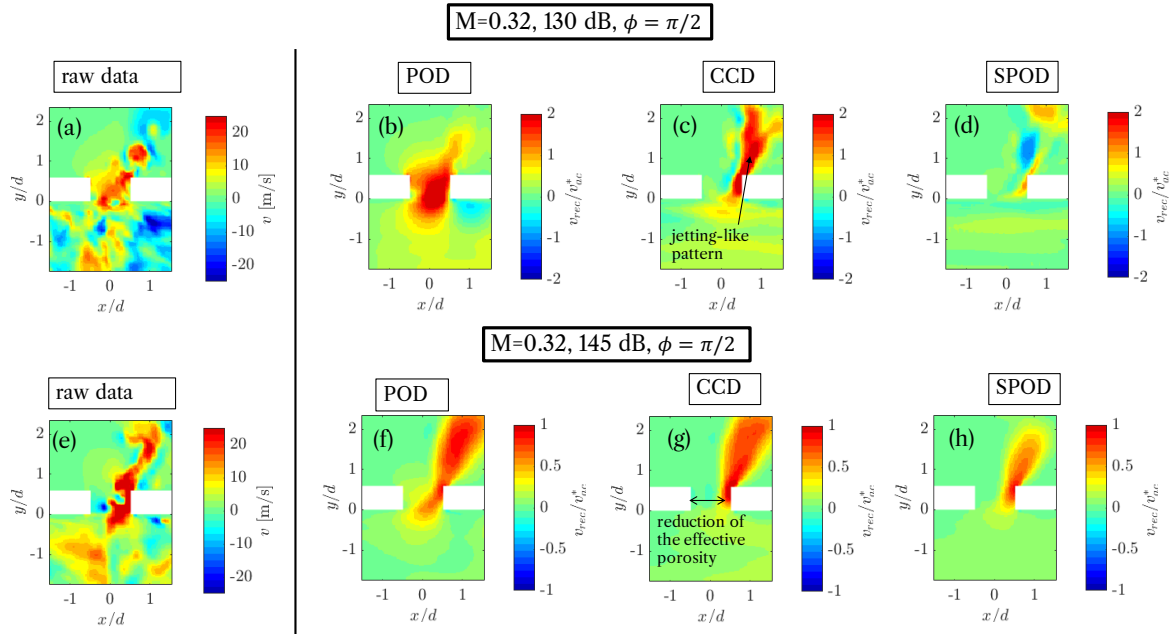


**Figure 3.** Contour of the reconstructed vertical velocity fluctuation,  $v$ , in the inflow phase ( $\phi = \pi/2$ ),  $M = 0.32$ ; first row 130 dB, second row 145 dB. Comparison of POD, CCD, SPOD; raw data are reported for clarity.

introducing the grazing flow, the spectra are dominated by the broadband effect of the turbulence at the low frequencies. At 130 dB, the peak at the forcing acoustic frequency does not emerge, but it is visible when increasing the SPL to 145 dB. As the source tone at 1.4 kHz does not emerge from the turbulence level at 130 dB, due to the limited AHFR, the SPOD works only if the forcing frequency is known a-priori.

## 4.2 Contours of the reconstructed vertical acoustic velocity

The contours of the normalized reconstructed vertical velocity are reported in figure 3 for both SPL at  $M = 0.32$ . For brevity, the contours reported are all related to the inflow phase ( $\phi = \pi/2$ ), namely when the flow enters inside the orifice (positive velocity) due to the effect of the acoustic waves. Along with the reconstructed velocity from the modal decompositions, it is reported a snapshot of the vertical velocity fluctuation in the inflow phase. It is clear that, in presence of grazing flow, the velocity field is polluted by the presence of the turbulent fluctuations in the vicinity of the orifice which are pushed inside the orifice by the acoustic induced velocity. In presence of graz-

ing flow, the equivalent porosity of the liner is reduced, and jet-like inflow/outflow velocities are evidenced in the downstream half of the orifice [24].

At 130 dB, as depicted in figure 3, the POD clearly does not show the formation of jetting-like motion in the downstream part of the orifice. For the POD, the reconstruction of the vertical velocity is highly influenced by the modes associated with the 14 kHz. The CCD seems to provide the neatest results but the magnitude of the acoustic velocity is larger compared with the reference used for scaling the results, while a lower velocity is deduced with SPOD.

At 145 dB the capability of all the eduction techniques to extract the acoustic velocity is improved compared with the 130 dB case. This is attributed to the larger acoustic-to-hydrodynamic fluctuation ratio. The POD shows traces of the flow feature attributed to the 14 kHz tone which occupy the entire orifice. For both SPL, SPOD and CCD results clearly evidence a region in the upstream half of the orifice where the flow is quasi-steady and the vertical velocity is negligible. This region corresponds to the formation of a vortex that limits the effective porosity of the orifice.

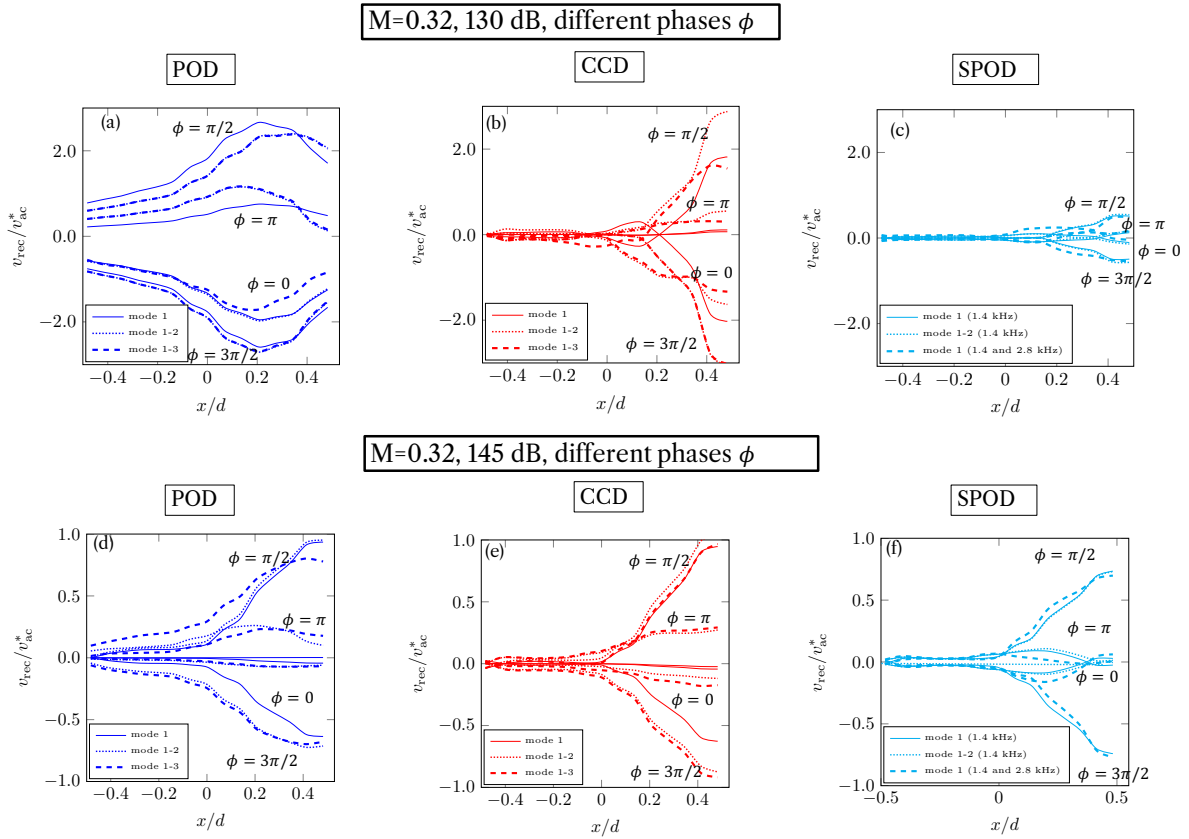


**Figure 4.** Reconstructed vertical velocity profiles at the center-line of the orifice using POD, CCD and SPOD at  $M = 0.32$ . First row 130 db, second row 145 db. Effect of the number of modes used for the reconstruction and the frequency band (SPOD), different phases  $\phi$  are reported.

### 4.3 Acoustic velocity profiles within the orifice at various phases

In figure 4 the acoustic velocity profiles, obtained at the centreline of the orifice, are shown at four phases:  $\phi = 0, \pi/2, \pi, 3\pi/2$ . The effect of changing the number of modes in the reduced order model is reported changing the line style as detailed in the legend.

The presence of the grazing turbulent flow generates a clear streamwise asymmetry in the inflow/outflow acoustic velocity profile. In the first half of the cavity the vertical velocity is negligible, thus the equivalent porosity of the orifice is then reduced by the presence of the grazing flow. This finding has been previously reported by several authors [20,24] and can be associated with the presence of a quasi-stationary vortex in the first portion of the orifice.

At 130 dB the acoustic profiles obtained with the dif-

ferent decomposition methods are different. This indicates a higher complexity and a lower reliability in the decomposition of acoustic and aerodynamic fields at lower acoustic-to-hydrodynamic fluctuation ratio. The POD results are influenced by the peak at 14 kHz that dominates the acoustic velocity. For this reason the profile exhibits a non-negligible vertical velocity in the upstream portion of the orifice in both inflow and outflow phases but also at  $\phi = 0$  and  $\phi = \pi$ . Based on the existing literature, this behaviour is not physical. The SPOD and CCD results are similar in shape but the maximum value of the acoustic velocity reconstructed with CCD is double the one reconstructed with SPOD.

The acoustic velocity profiles at 145 dB obtained with the different techniques are very similar. This is due to a larger AHFR and indicates a clear predominance of acous-



# FORUM ACUSTICUM EURONOISE 2025

tic induced flow with respect to the grazing flow entering inside the orifice. The effect of changing the number of modes is almost negligible for all the technique considered excluding the POD where the third mode pollutes the results. This discrepancy is due to the fact that the third POD mode at 145 dB might keep a trace of the 14 kHz leading to an increased vertical velocity along the centre-line of the orifice.

## 5. CONCLUSIONS

Three different methods, POD, CCD and SPOD, are tested to separate the vertical velocity field into a turbulent and an acoustic-induced components. The methodologies proposed herein can be of wide applicability for experimental and numerical data. The decompositions are tested on a numerical database that represents an orifice of an acoustic liner subjected to a grazing flow and grazing acoustic forcing. For acoustic liners a correct evaluation of the acoustic velocity is of pivotal interest in the computation of impedance.

The first conclusion is that the eduction of the acoustic velocity using the methods proposed herein is highly influenced by the AHFR, namely by the magnitude of the acoustic induced field with respect to the aerodynamic fluctuation due to the turbulence. In presence of grazing flow all the decomposition methods show almost identical results for the high SPL condition, while at low SPL all the results differs.

The POD is the method that most suffer from the low magnitude of acoustic-induced field with respect to the broad level of turbulence. As POD ranks the modes by energetic content, it is highly influenced by the presence of high energy associated with spurious frequencies different from the acoustic ones. These frequencies might be physical, as in the current investigation the 14 kHz tone, or due to noise in experimental data.

SPOD has the advantage of highlighting energetically relevant features and how they distribute on the frequencies. A fundamental limitation of SPOD is that, as it evaluates the acoustic-induced field by reconstructing the SPOD spectrum on a certain frequencies band, the acoustic-induced field contains the hydrodynamic fluctuations due to the turbulence at the same frequency of the acoustic source. This contribution is expected to be non negligible as the acoustic field is expected to interact with the turbulent field and modulate it. One other important limitation is that the frequency at which the acoustic field is reconstructed needs to be known a-priori. If the AHFR

is high, for the SPOD, the frequency can be identified by the inspection of the spectrum while at low AHFR the acoustic induced contribution might not emerge in the energy spectrum.

CCD and POD automatically capture non-linear effects in higher order modes. The SPOD, by applying a Fourier decomposition treats intrinsically the system as linear. This has the advantage of decomposing linearly the acoustic velocity generated by the sound into a contribution of different frequencies. If the non-linear effects have to be included in the acoustic-induced field, one needs to know a-priori the frequency of interests and the non-linear frequencies such as the harmonics. One advantage of CCD is that it does not require any arbitrary filtering (as the choice of the acoustic frequency or frequency band). However, CCD requires a reference signal so it is more suited if the objective is to study the acoustic field induced by a known reference source. In addition the choice of the position of the reference signal is arbitrary and might alter the results.

All the methods are highly influenced by the number of samples of the dataset. If the signal is too short, CCD and POD are not able to separate in different modes the non linear effects, while SPOD forces the signal to separate into multiple frequencies and allows to reconstruct the velocity field based on one particular frequency band. However, for SPOD the duration of the signal influences the frequency and the modal resolution.

## 6. ACKNOWLEDGEMENTS

The work of F. Scarano, A. Paduano and F. Avalone is funded by the European Union (ERC, LINING, 101075903). Views and opinions expressed are however those of the author(s) only and do not necessarily reflect those of the European Union or the European Research Council. Neither the European Union nor the granting authority can be held responsible for them.

## 7. REFERENCES

- [1] R. E. A. Arndt, D. F. Long, and M. N. Glauser, "The proper orthogonal decomposition of pressure fluctuations surrounding a turbulent jet," *Journal of Fluid Mechanics*, vol. 340, p. 1–33, 1997.
- [2] J. E. F. Williams, "Hydrodynamic noise," *Annual Review of Fluid Mechanics*, vol. 1, no. Volume 1, 1969, pp. 197–222, 1969.





# FORUM ACUSTICUM EURONOISE 2025

- [3] M. Mancinelli, T. Pagliaroli, A. Di Marco, R. Camussi, and T. Castelain, “Wavelet decomposition of hydrodynamic and acoustic pressures in the near field of the jet,” *Journal of Fluid Mechanics*, vol. 813, pp. 716–749, Feb. 2017.
- [4] B. Arguillat, D. Ricot, C. Bailly, and G. Robert, “Measured wavenumber: Frequency spectrum associated with acoustic and aerodynamic wall pressure fluctuations,” *The Journal of the Acoustical Society of America*, vol. 128, pp. 1647–1655, Oct. 2010. [\\_eprint: https://pubs.aip.org/asa/jasa/article-pdf/128/4/1647/13782828/1647\\_1\\_online.pdf](https://pubs.aip.org/asa/jasa/article-pdf/128/4/1647/13782828/1647_1_online.pdf).
- [5] S. Schoder, K. Roppert, and M. Kaltenbacher, “Post-processing of Direct Aeroacoustic Simulations Using Helmholtz Decomposition,” *AIAA Journal*, vol. 58, pp. 3019–3027, July 2020.
- [6] P. J. Schmid, “Dynamic mode decomposition of numerical and experimental data,” *Journal of Fluid Mechanics*, vol. 656, pp. 5–28, Aug. 2010.
- [7] S. Grizzi and R. Camussi, “Wavelet analysis of near-field pressure fluctuations generated by a subsonic jet,” *Journal of Fluid Mechanics*, vol. 698, pp. 93–124, May 2012.
- [8] B. Lyu, “Canonical correlation decomposition of numerical and experimental data for observable diagnosis,” in *30th AIAA/CEAS Aeroacoustics Conference*, pp. AIAA 2024–3206, 2024.
- [9] J. Lumley, “The structure of inhomogeneous turbulent flows,” *Atmospheric Turbulence and Radio Wave Propagation*, pp. 166–177, 1967.
- [10] G. Berkooz, P. Holmes, and J. L. Lumley, “The proper orthogonal decomposition in the analysis of turbulent flows,” *Annual Review of Fluid Mechanics*, vol. 25, no. Volume 25, 1993, pp. 539–575, 1993.
- [11] J. Weiss, “A Tutorial on the Proper Orthogonal Decomposition,” in *AIAA Aviation 2019 Forum*, (Dallas, Texas), American Institute of Aeronautics and Astronautics, June 2019.
- [12] O. T. Schmidt and T. Colonius, “Guide to Spectral Proper Orthogonal Decomposition,” *AIAA Journal*, vol. 58, pp. 1023–1033, Mar. 2020.
- [13] P. Morse, K. Ingard, and P. Morse, *Theoretical Acoustics: By Philip M. Morse and K. Uno Ingard*. McGraw-Hill, 1968.
- [14] A. Paduano, F. Scarano, J. Cordioli, D. Casalino, and F. Avallone, “Description of the aerodynamic and acoustic flow fields within cavity of acoustic liner.” to be submitted, 2025.
- [15] X. He and L. S. Luo, “Theory of the lattice Boltzmann method: From the Boltzmann equation to the lattice Boltzmann equation,” *Physical Review E - Statistical Physics, Plasmas, Fluids, and Related Interdisciplinary Topics*, vol. 55, no. 6, 1997.
- [16] Y. H. Qian, D. D’Humières, and P. Lallemand, “Lattice bgk models for navier-stokes equation,” *EPL*, vol. 17, no. 6, 1992.
- [17] V. Yakhot and S. A. Orszag, “Renormalization-group analysis of turbulence,” *Physical Review Letters*, vol. 57, no. 14, 1986.
- [18] L. A. Bonomo, A. M. Spillere, and J. A. Cordioli, “Parametric uncertainty analysis for impedance education based on prony’s method,” *AIAA Journal*, vol. 58, no. 8, 2020.
- [19] C. K. W. Tam and K. A. Kurbatskii, “Microfluid Dynamics and Acoustics of Resonant Liners,” *AIAA Journal*, vol. 38, pp. 1331–1339, Aug. 2000.
- [20] O. Léon, F. Méry, E. Piot, and C. Conte, “Near-wall aerodynamic response of an acoustic liner to harmonic excitation with grazing flow,” *Experiments in Fluids*, vol. 60, 9 2019.
- [21] C. K. Tam, H. Ju, M. Jones, W. Watson, and T. Parrott, “A computational and experimental study of resonators in three dimensions,” *Journal of Sound and Vibration*, vol. 329, pp. 5164–5193, Nov. 2010.
- [22] R. L. Panton and J. M. Miller, “Resonant frequencies of cylindrical Helmholtz resonators,” *The Journal of the Acoustical Society of America*, vol. 57, pp. 1533–1535, June 1975. [\\_eprint: https://pubs.aip.org/asa/jasa/article-pdf/57/6/1533/11595089/1533\\_1\\_online.pdf](https://pubs.aip.org/asa/jasa/article-pdf/57/6/1533/11595089/1533_1_online.pdf).
- [23] G. Dacome, R. Siebols, and W. Baars, “Small-scale helmholtz resonators with grazing turbulent boundary layer flow,” *Journal of Turbulence*, vol. 25, no. 12, pp. 461–481, 2024.
- [24] Q. Zhang and D. J. Bodony, “Numerical investigation of a honeycomb liner grazed by laminar and turbulent boundary layers,” *Journal of Fluid Mechanics*, vol. 792, pp. 936–980, 3 2016.

